Journal of Power Sources 196 (2011) 2171–2178

Contents lists available at ScienceDirect

Journal of Power Sources

journal homepage: www.elsevier.com/locate/jpowsour

Improved synthesis of a highly fluorinated boronic ester as dual functional additive for lithium-ion batteries☆

Wei Weng[a], Zhengcheng Zhang[a,*], John A. Schlueter[b], Paul C. Redfern[a], Larry A. Curtiss[b,c], Khalil Amine[a,**]

[a] Chemical Sciences and Engineering Division, Argonne National Laboratory, 9700 South Cass Avenue, Argonne, IL 60439, USA
[b] Materials Science Division, Argonne National Laboratory, 9700 South Cass Avenue, Argonne, IL 60439, USA
[c] Center for Nanoscale Materials, Argonne National Laboratory, 9700 South Cass Avenue, Argonne, IL 60439, USA

ARTICLE INFO

Article history:
Received 12 August 2010
Accepted 29 September 2010
Available online 7 October 2010

Keywords:
Tetrafluorocatechol
Single-crystal X-ray diffraction
Lithium-ion batteries
Overcharge protection

ABSTRACT

The electrolyte additive 2-(pentafluorophenyl)-tetrafluoro-1,3,2-benzodioxaborole (PFPTFBB, **1**) was found to have a reversible redox potential at 4.43 V vs. Li^+/Li. This compound can function as an overcharge protection additive as well as anion receptor for lithium-ion batteries. It has drawn a great deal of interest from industry, but its use in relatively large quantities is limited by the production challenges of tetrafluorocatechol (TFC, **3**), which is the key starting chemical for the synthesis of PFPTFBB. As part of a continuous effort in our research toward improving the safety of lithium-ion batteries, we have performed the synthesis of TFC and optimized its synthesis process. The X-ray single-crystal structures of TFC and the intermediate product 5,6,7,8-tetrafluoro-1,4-benzodioxane (**4**) during the process of PFPTFBB synthesis are reported for the first time. Also presented is the lithium ion cell performance of PFPTFBB as redox shuttle in various electrolyte systems.

1. Introduction

Aromatic boron esters have recently received much attention within the lithium-ion battery community. These molecules were proposed as promising additives for nonaqueous electrolytes. They can function as anion receptors to dissolve LiF formed during the operation of lithium-ion batteries and thus improve the properties of commercial electrolytes [1]. Recently, our group reported that the fluorinated boronate ester, 2-(pentafluorophenyl)-tetrafluoro-1,3,2-benzodioxaborole (PFPTFBB, **1**), can behave both as anion receptor and as a redox shuttle for overcharge protection of lithium-ion batteries [2]. We found that **1** has a reversible redox potential at 4.43 V vs. Li^+/Li. This potential is high enough to provide overcharge protection for most 4.2 V positive electrode materials. In cell tests, we were able to achieve 170 cycles of 100% overcharge while **1** functioned as an active redox shuttle.

As shown in Scheme 1, PFPTFBB (**1**) can be prepared from the condensation reaction of pentafluorobenzene boronic acid (**2**) and TFC (**3**) [1,2]. The reaction was driven to completion by azeotropic distillation to remove the water byproduct from the reaction. The starting material **2** is widely available from commercial suppliers due to its easy preparation and wide application as a useful synthon in cross-coupling reactions. However, the TFC supply is very limited, and the samples that we obtained from a few commercial sources were found to contain a large amount of impurity, which was identified to be 1,2-diphenylethane. Fig. 1 is the ^{1}H NMR spectra of TFC (pure) and TFC sample obtained from a commercial supplier. The singlet at 3.0 ppm and multiplet at 7.2–7.4 ppm can be ascribed to the CH_2 and aromatic protons in 1,2-diphenylethane. Interestingly, TFC and 1,2-diphenylethane have the same molecular weight (MW = 182), therefore, particular attention needs to be paid when using gas chromatography/mass spectrometry or other mass methods as the only routine quality control analysis.

The intermediate TFC can be synthesized in a three-step sequence starting from hexafluorobenzene, as reported by Burdon et al. [3] and then confirmed by Willis et al. [4], in less than 10% yield. Gores et al. reported the synthesis of TFC from pentafluorophenol in three steps with slightly better yields [5]. This method involves the use of ethylene oxide, which is a flammable gas

☆ The submitted article has been created by UChicago Argonne, LLC, Operator of Argonne National Laboratory ("Argonne"). Argonne, a U.S. Department of Energy Office of Science Laboratory, is operated under Contract No. DE-AC02-06CH11357. The U.S. Government retains for itself, and others acting on its behalf, a paid-up nonexclusive, irrevocable worldwide license in said article to reproduce, prepare derivative works, distribute copies to the public, and perform publicly and display publicly, by or on behalf of the government.

* Corresponding author at: Argonne National Laboratory, Chemical Sciences and Engineering Division, 9700 South Cass Avenue, Building 205, Lemont, IL 60439, USA. Tel.: +1 630 252 7868; fax: +1 630 972 4440.
** Corresponding author. Tel.: +1 630 252 3838; fax: +1 630 972 4672.
E-mail addresses: zzhang@anl.gov (Z. Zhang), amine@anl.gov (K. Amine).

0378-7753/$ – see front matter © 2010 Elsevier B.V. All rights reserved.
doi:10.1016/j.jpowsour.2010.09.110

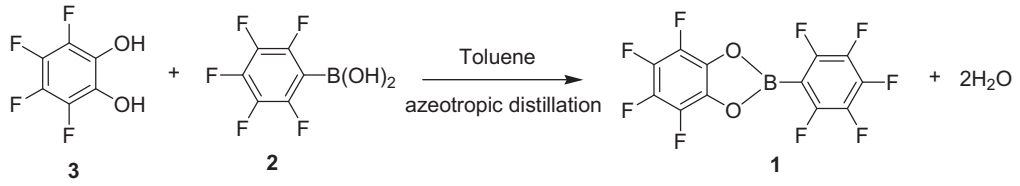

Scheme 1. Synthesis of PFPTFBB (**1**).

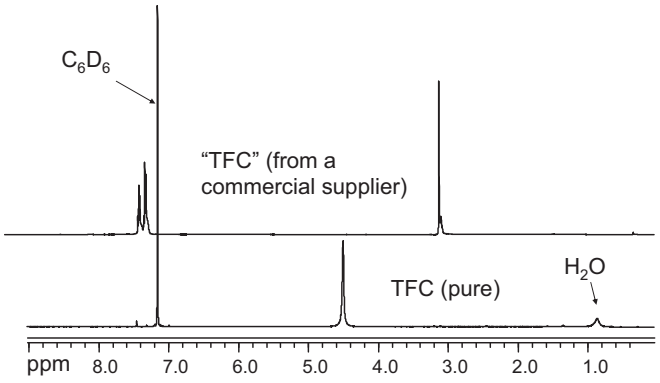

Fig. 1. Stacked ^{1}H NMR spectra of synthesized TFC (pure) and TFC sample obtained from a commercial supplier.

and very difficult to handle. Therefore, we performed the synthesis of TFC with improved yield and reported for the first time the X-ray structures of TFC and the intermediate product 5,6,7,8-tetrafluoro-(1,4)-benzodioxane (**4**). The electrochemical properties of **4** and final product PFPTFBB were studied by cyclic voltammetry. We also performed density functional theory (DFT) calculations to probe the optimized structures and the oxidation potentials. These results were in good agreement with the experimental data. The overcharge protection performance of PFPTFBB in mixed carbonate-based electrolytes complexed with different lithium salts was also evaluated.

2. Experimental

2.1. Materials and methods

All chemicals were purchased from commercial suppliers and used without further purification. ^{1}H and ^{13}C nuclear magnetic resonance (NMR) spectra were recorded on a Bruker 500 MHz Fourier-transform NMR spectrometer. Electrospray mass spectra (ESI-MS) were recorded on freshly prepared samples (ca. 1 mg mL^{-1} in CH_2Cl_2) using an Agilent 1100 LC-MSD spectrometer incorporating a quadrupole mass filter with an m/z range of 0–3000.

2.2. Synthesis

The intermediates 2-pentafluorophenoxyethyl alcohol (**5**), 5,6,7,8-tetrafluoro-(1,4)-benzodioxane (**4**), and 3,4,5,6-tetrafluoropyrocatechol (**3**) were synthesized according to the Scheme 2.

2.2.1. 2-Pentafluorophenoxyethyl alcohol (*5*)

C_6F_6 (100 g, 62 mL) was added to KOH (29 g) suspended in ethylene glycol (320 mL). The reaction mixture was heated to 110 °C for 4 h. After cooling down to room temperature, the reaction mixture was diluted with water and acidified with H_2SO_4. The organic materials were extracted with diethyl ether and dried over anhydrous magnesium sulfate. After filtration, the solvent was removed by rotary evaporator. The title compound was obtained as colorless oil from fraction of 80–85 °C at 1 mmHg during vacuum distillation. The yield was 53 g (42%). ^{1}H NMR ($CDCl_3$): δ 4.27 (t, J = 5 Hz), 3.93 (t, J = 5 Hz), 3.74 (s, –OH). ^{13}C NMR ($CDCl_3$): δ 141.6 (dm, $^{1}J_{C-F}$ = 241 Hz), 137.9 (dt, $^{1}J_{C-F}$ = 247 Hz, $^{2}J_{C-F}$ = 14 Hz), 137.5 (dt, $^{1}J_{C-F}$ = 250 Hz, $^{2}J_{C-F}$ = 14 Hz), 133.5 (t, $^{2}J_{C-F}$ = 12 Hz), 76.7 (s), 61.4 (s).

2.2.2. 5,6,7,8-Tetrafluoro-(1,4)-benzodioxane (*4*)

A mixture of **5** (52 g, 0.23 mol) and K_2CO_3 (57 g) in anhydrous dimethylformamide (350 mL) was refluxed under N_2 for 20 h. After cooling down to temperature, the mixture was poured into 1.5 L ice water. The precipitate was collected by filtration and thoroughly washed with water. The crude product **4** can be further purified by flash chromatography (SiO_2, hexane/ethyl acetate = 10:1). The yield was 20 g (43%). X-ray quality crystals were obtained

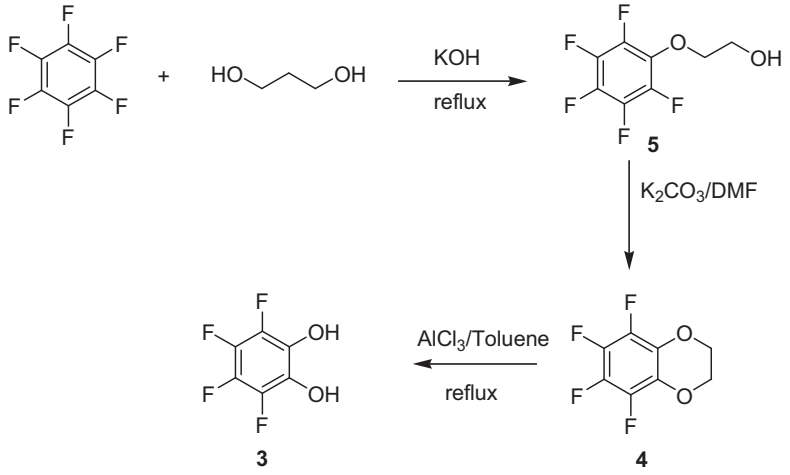

Scheme 2. Synthesis of TFC (**3**).

from slow evaporation of **4** in a 10:1 mixture of hexane and ethyl acetate. ^{1}H NMR ($CDCl_3$): δ 4.27 (t, J = 5 Hz), 3.93 (t, J = 5 Hz), 3.74 (s, –OH). ^{13}C NMR ($CDCl_3$): δ 141.6 (dm, $^1J_{C-F}$ = 241 Hz), 137.9 (dt, $^1J_{C-F}$ = 247 Hz, $^2J_{C-F}$ = 14 Hz), 137.5 (dt, $^1J_{C-F}$ = 250 Hz, $^2J_{C-F}$ = 14 Hz), 133.5 (t, $^2J_{C-F}$ = 12 Hz), 76.7 (s), 61.4(s).

2.2.3. 3,4,5,6-Tetrafluorocatechol (**3**)

To a solution of **4** (10 g, 0.048 mol) in dry benzene (400 mL) was added anhydrous $AlCl_3$ (40 g). The reaction mixture was heated to 85 °C and stirred for 6 h. After cooling down to room temperature, the reaction mixture was quenched with ice/H_2O and filtered. The filtrate was acidified with H_2SO_4, and organic materials were extracted with diethyl ether. The organic layer was dried by anhydrous $MgSO_4$ and concentrated to a viscous oil, which was purified by column chromatography (SiO_2, CH_2Cl_2/ethyl acetate = 10:1) to yield **3** as an off-white oil. The crude oil was allowed to sit for 2 days to solidify. The resulting dark gray solid can further be purified by vacuum sublimation at 60 °C (1 mmHg) to generate **3** as a white crystalline solid (using a cryogenic sublimation apparatus from Chemglass, with dry ice/acetone in the cold finger). The yield was 2.5 g (28%). ^{1}H NMR ($CDCl_3$): δ 5.47 (s, –OH). ^{13}C NMR ($CDCl_3$): δ 137.5 (dm, $^1J_{C-F}$ = 246 Hz), 135.4 (dm, $^1J_{C-F}$ = 247 Hz), 129.6 (d, $^2J_{C-F}$ = 14 Hz, C–O).

2.2.4. 2-(Pentafluorophenyl)-tetrafluoro-1,3,2-benzodioxaborole (**1**)

The redox shuttle additive **1** was synthesized according to the Scheme 1. TFC (**3**) (7.16 g, 0.039 mol) and pentafluorobenzene boronic acid (**2**) (8.34 g, 0.039 mol) were mixed in 50 mL anhydrous toluene. The mixture was heated up to reflux and maintained at this temperature for 12 h. The water generated during the reaction was removed by azeotropic distillation. After cooling down to room temperature, the solvent was removed under reduced pressure. The residue was sublimed at 110 °C and 0.1 mmHg to afford the title compound. The yield was 11.5 g (82%). ^{19}F (d_6-DMSO): δ −139.2 (m, 2F), −154.9 (q, 1F), −162.6 (m, 2F), −164.4 (t, 2F), −173.5 (t, 2F).

2.3. Crystal structure determination by single-crystal X-ray diffraction

Colorless crystals of **3** and **4** were mounted onto the tip of a MiTeGen micromount with Paratone N oil and placed on a Bruker APEX II 3-circle diffractometer equipped with an APEX II detector. The crystal temperature was maintained at 100(2) K through use of an Oxford Cryostream 700 Plus LT device. Attempts to collect data at room temperature were unsuccessful due to sublimation of the crystal. The analysis was carried out using MoKα radiation (λ = 0.71073 Å) with a frame exposure time of 30 s and a detector distance of 5.00 cm. Three hemispheres were collected with 0.30° ω scans. The raw intensity data were corrected for absorption (SADABS) [6]. The structure was solved and refined by using SHELXTL [7]. A direct-method calculation provided most of atomic positions from the e-map. Full-matrix least squares/difference Fourier cycles were performed to locate the remaining atoms. All non-hydrogen atoms were refined with anisotropic displacement parameters. Hydrogen atoms from water molecules were located from a difference Fourier map. All the other hydrogen atoms were placed in ideal positions and refined as "riding atoms" with relative isotropic displacement parameters. Structural and refinement parameters are provided in Table 1.

2.4. Electrochemical property

Cyclic voltammetry experiments using a Solartron Analytical 1470E system were performed in custom-made three-electrode cells with a 1 mm-diameter Pt working electrode, a Li metal reference electrode, and a Li counter electrode. The electrolyte was 1.2 M $LiPF_6$ in a mixture of ethylene carbonate and ethyl methyl carbonate (EC/EMC) in a volume ratio of 3:7. PFPTFBB or **4** was added to the electrolyte in a concentration of 0.1 M. The sweep rate was varied from 10 to 200 mV s^{-1}.

Overcharge tests were conducted in 2032 coin-type cells of $Li_4Ti_5O_{12}$ (LTO)/$LiFePO_4$. The electrolyte was 1.2 M $LiPF_6$ in 3:7 EC/EMC containing 1 wt% of PFPTFBB. The cells were charged at a constant current until a specific upper cutoff voltage was reached (normally 3.45 V vs. $Li_4Ti_5O_{12}$).

Table 1
Crystal data and structure refinement of complexes **3** and **4**.

	3	**4**
Formula	$C_6H_4F_4O_3$	$C_8H_4F_4O_2$
MW	200.09	208.11
Cryst. syst.	Monoclinic	
T/K	100(2)	
Wavelength	0.71073 Å	
Space group	$P2(1)/n$	$C2/c$
a/Å	14.2386(7)	4.2660(2)
b/Å	6.6798(3)	17.3259(6)
c/Å	14.8002(8)	9.8660(4)
β/°	103.873(2)	97.423(1)
V/Å^3	1366.60(12)	723.11(5)
Z	8	4
ρ/g cm^{-3}	1.945	1.912
μ/mm^{-1}	0.220	0.202
F(0 0 0)	800	416
GoF	0.777	1.190
$R1$, $wR2$ [$I > 2\sigma(I)$]	0.0293, 0.0755	0.0491, 0.1293
$R1$, $wR2$ (all data)	0.0315, 0.0775	0.0495, 0.1297

$$R1 = \frac{\sum ||F_o| - |F_c||}{\sum |F_o|}; \quad wR2 = \left[\frac{\sum w(F_o^2 - F_c^2)^2}{\sum w(F_o^2)^2}\right]^{1/2}; \quad \text{GoF} = \left[\frac{\sum w(F_o^2 - F_c^2)^2}{N_{obs} - N_{var}}\right]^{1/2}$$

3. Results and discussion

3.1. Synthesis of TFC (**3**)

As shown in Scheme 2, the synthesis of **5** is straightforward and the yield is moderate (45–50%). The final product contains a small amount of ethylene glycol, evidenced by a sharp ^{1}H NMR signal at 3.7 ppm for the ethylene CH_2–CH_2 group. No further purification step was taken. The cyclization reaction of **5** under basic condition occurs at high temperature. In Burdon's method [3], the reaction mixture was quenched with ice water and then acidified to afford **4** as a white solid. However, we found the addition of acid results in the formation of viscous oil, not the white solid. In our synthesis, **4** can be simply obtained by filtration of the quenched mixture without adjusting the pH. Crude **4** needs to be washed thoroughly with water to remove inorganic salts and pentafluorophenol byproduct. In the final step, the isolation of **3** from the major byproduct bibenzyl formed through the $AlCl_3$ catalyzed Friedel–Crafts reaction of benzene and in situ formed ethylene dichloride. Repeated sublimation procedures seem not to be able to separate product **3** from the bibenzyl product. However, **3** can be obtained in pure form by flash column chromatography using a mixture of CH_2Cl_2 and ethyl acetate as elute.

3.2. Crystal structures

3.2.1. Crystal structure of **4**

The molecular structure of **4** is illustrated in Fig. 2, and selected bond distance and angles are provided in Table 2. In the solid state, the six-membered 1,4-dioxane ring fused to the benzene ring adopts a half-chair conformation. The two oxygen atoms are nearly

Table 2
Selected bond lengths (Å) and bond angles (°) for **4** and **3**. Calculated values from B3LYP/6-31G* in square brackets.

Complex 4			
C1–O1	1.4468(11) [1.431]	C1–C1[a]	1.5123(19) [1.520]
C2–O1	1.3609(10) [1.367]	C2–C3	1.3929(11) [1.398]
C2–C2[a]	1.3999(16) [1.404]	C3–F1	1.3411(10) [1.340]
C3–C4	1.3807(11) [1.390]	C4–F2	1.3426(9) [1.340]
C4–C4[a]	1.3870(17) [1.394]	C2–O1–C1	112.18(7)
O1–C1–C1[a]	109.90(7)	O1–C2–C3	117.95(8)
O1–C2–C2[a]	122.93(4)	C3–C2–C2[a]	119.11(5)
F1–C3–C4	119.53(7)	F1–C3–C2	119.35(7)
C4–C3–C2	121.12(9)	F2–C4–C3	120.51(8)
F2–C4–C4[a]	119.77(5)	C3–C4–C4[a]	119.72(5)
C1–O1–C2–C2[a]	15.09 [16.0]	C1–O1–C2–C3	165.90 [164.2]
Complex **3**			
C1–C6	1.381(2)	C11–C16	1.379(2)
C1–C2	1.383(2)	C11–C12	1.382(2)
C2–O2	1.3617(18)	C12–O12	1.3622(17)
C2–C3	1.400(2)	C12–C13	1.399(2)
C3–O3	1.3485(18)	C13–O13	1.3620(17)
C3–C4	1.386(2)	C13–C14	1.385(2)
C4–F4	1.3507(17)	C14–F14	1.3505(16)
C4–C5	1.379(2)	C14–C15	1.377(2)
C5–F5	1.3436(17)	C15–F15	1.3425(17)
C5–C6	1.380(2)	C15–C16	1.380(2)
C6–F6	1.3408(17)	C16–F16	1.3398(17)
F1–C1–C6	118.94(13)	F1–C1–C6	118.94(13)
F1–C1–C2	118.84(13)	F1–C1–C2	118.84(13)
C6–C1–C2	122.22(14)	C6–C1–C2	122.22(14)
O2–C2–C1	118.14(13)	O2–C2–C1	118.14(13)
O2–C2–C3	123.08(13)	O2–C2–C3	123.08(13)
C1–C2–C3	118.77(14)	C1–C2–C3	118.77(14)
O3–C3–C4	124.09(13)	O3–C3–C4	124.09(13)
O3–C3–C2	117.60(13)	O3–C3–C2	117.60(13)
C4–C3–C2	118.29(13)	C4–C3–C2	118.29(13)
F4–C4–C5	119.28(13)	F4–C4–C5	119.28(13)
F4–C4–C3	118.34(13)	F4–C4–C3	118.34(13)
C5–C4–C3	122.37(14)	C5–C4–C3	122.37(14)
F5–C5–C4	120.12(14)	F5–C5–C4	120.12(14)
F5–C5–C6	120.66(14)	F5–C5–C6	120.66(14)
C4–C5–C6	119.20(14)	C4–C5–C6	119.20(14)
F6–C6–C5	121.11(14)	F6–C6–C5	121.11(14)
F6–C6–C1	119.82(14)	F6–C6–C1	119.82(14)
C5–C6–C1	119.07(14)	C5–C6–C1	119.07(14)

[a] $-x, y, -z+1/2$.

coplanar with the benzene ring with one 0.056(1) Å above and the other equally below the best plane through the aromatic ring. The carbon atoms of the ethylene group lie 0.402(1) Å above and below this plane. The C–F distances are 1.3411(10) and 1.3426(9), close to the C–F distances observed in polyfluorinated dibenzo-*p*-dioxins [8,9]. The C2–O1 distance of 1.3609(10) Å is significantly shorter than the C1–O1 bond length of 1.4468(11) Å due to the different hybridization states of carbon. Also, the relatively shorter distance of C2–O1 in **4** compared to that of its non-fluorinated benzodioxane derivative **6** (Fig. 3) indicates stronger conjugation effects between the oxygen and the aryl rings. This effect can be explained by the electron withdrawing property of fluorine atoms, which stabilize the partial negative charge in the resonance structures [10].

Molecules of **4** are canted 34.19(3)° with respect to the (1 0 0) plane. The aromatic ring centroid separation is equivalent to the *a*-axis, with the perpendicular separation between these rings being 3.189 Å and a slippage of 2.833 Å. As illustrated in Fig. 4, these molecules pack with fluorophilic layers parallel to (1 0 1) at $y = 0.5$. The shortest intermolecular F···F interaction is 2.7209(12) Å [11,12].

3.2.2. Crystal structure of **3**·(H_2O)

Drawings of the two crystallographically independent molecules of **3** and two water molecules in the asymmetric unit of **3**·(H_2O) are provided in Fig. 5. Selected bond distances and angles are provided in Table 2. Within the aromatic rings, the longest C–C bonds are those between the hydroxyl carbon atoms, with bond distances of 1.400(2) and 1.399(2) Å. The remaining C–C bonds range from 1.377(2) to 1.383(2) Å. The C–F bonds range from 1.340(2) to 1.352(2) Å, with C–O bonds ranging from 1.349(2) to 1.362(2) Å. As expected, the aromatic rings are planar, with the largest deviation from the carbon plane being 0.018(1) Å. Oxygen atoms O2 and O3 reside 0.063(2) and 0.068(2) Å above and below the aromatic ring, respectively. As tabulated in Table 3, extensive hydrogen bonding interactions occur between the two molecules of **3** and the cocrystallized water. As illustrated in Fig. 6, this

Table 3
Hydrogen bonds for **3**·(H_2O) [Å and°].

D–H···A	*d*(D–H)	*d*(H···A)	*d*(D···A)	<(DHA)
O2–H2···O21	0.73(2)	2.04(2)	2.755(2)	167(2)
O3–H3···O20	0.79(2)	1.92(2)	2.697(2)	169(2)
O12–H12···O2[a]	0.76(2)	2.09(2)	2.835(2)	167(2)
O13–H13···O21	0.78(2)	1.98(2)	2.749(2)	169(2)
O20–H20A···O13[b]	0.82(2)	2.06(2)	2.869(2)	173(2)
O20–H20B···O12	0.79(2)	2.18(2)	2.962(2)	167(2)
O21–H21A···O20[c]	0.81(2)	1.96(2)	2.760(2)	170(2)

Symmetry transformations used to generate equivalent atoms:
[a] $x+1/2, -y+1/2, z+1/2$.
[b] $-x+2, -y, -z+1$.
[c] $-x+2, -y+1, -z+1$.

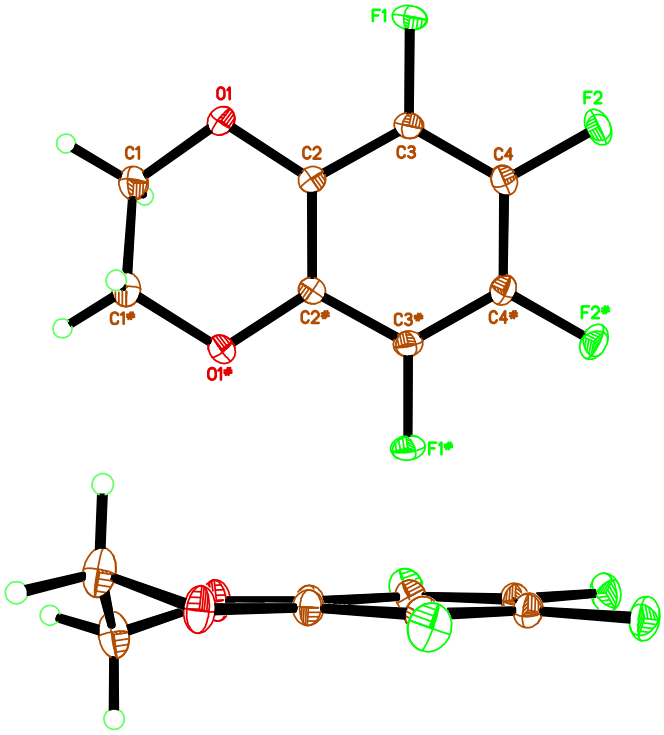

Fig. 2. Thermal ellipsoid plot for **4**. Ellipsoids are drawn at 50% probability. Hydrogen atoms are depicted as spheres of arbitrary radius. # $-x, y, 1/2-z$.

arrangement results in a layered structure with hydrogen bonded planes running parallel to (−1 0 1) separated by fluorophillic planes with intermolecular F···F interactions as short as 2.6625(12) Å. Because of this segregation, there are no significant hydrogen bonding interactions between hydroxyl or water and fluorine.

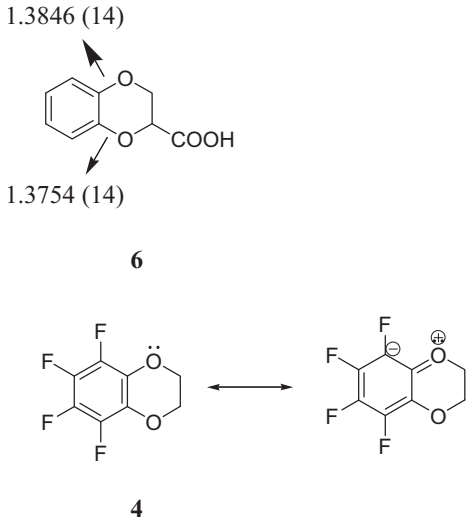

Fig. 3. Resonance structures of **4**.

The NMR chemical shift of crystallized water in a solution of **3**·(H_2O) in $CDCl_3$ implies the hydrogen bonding of **3** and water molecules in the solution phase. ^{1}H NMR resonance of crystallized water appears at 2.22 ppm in the $CDCl_3$ solution of **3**, quite downfield to the proton NMR signals of water in pure $CDCl_3$ (1.56 ppm). This difference can be explained by the fact that the hydrogen bonding in **3**·(H_2O) causes less shielding on the hydrogen atoms in water molecule.

3.3. Redox potential of *4*

Fig. 7 shows cyclic voltammograms for 0.05 M of **4** in 1.2 M $LiPF_6$ in EC/EMC (3/7 by volume) with sweep rates of 10, 20, 50, 100, and 200 mV s^{-1}. A well-defined reversible redox couple is observed. The

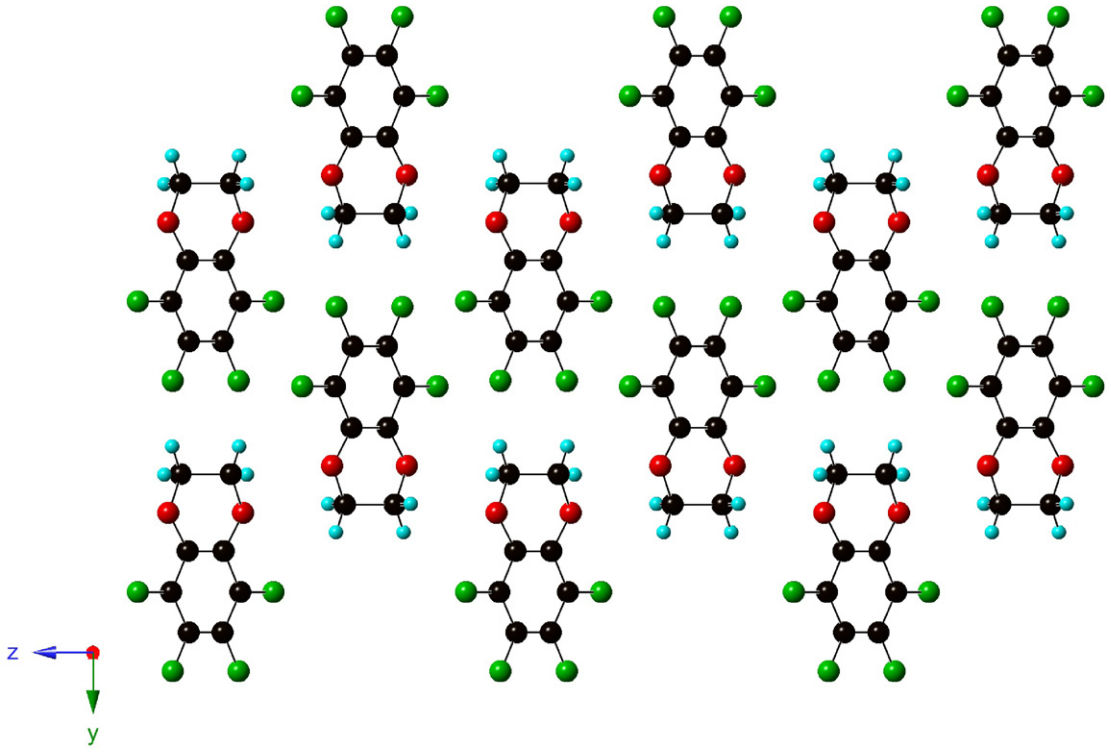

Fig. 4. Packing diagram for **4**.

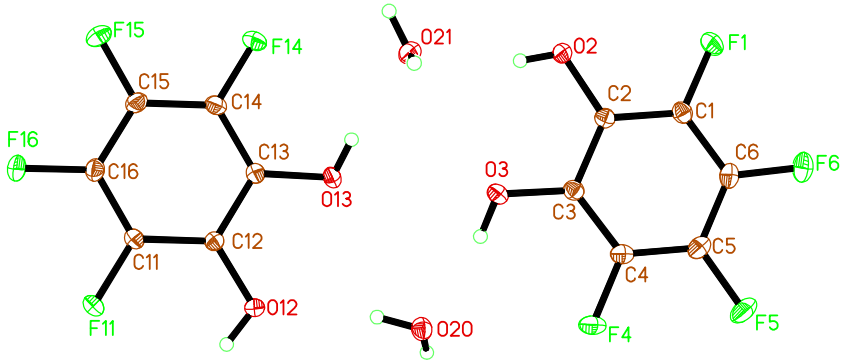

Fig. 5. Thermal ellipsoid plot for **3**·(H_2O). Ellipsoids are drawn at 50% probability. Hydrogen atoms are depicted as spheres of arbitrary radius.

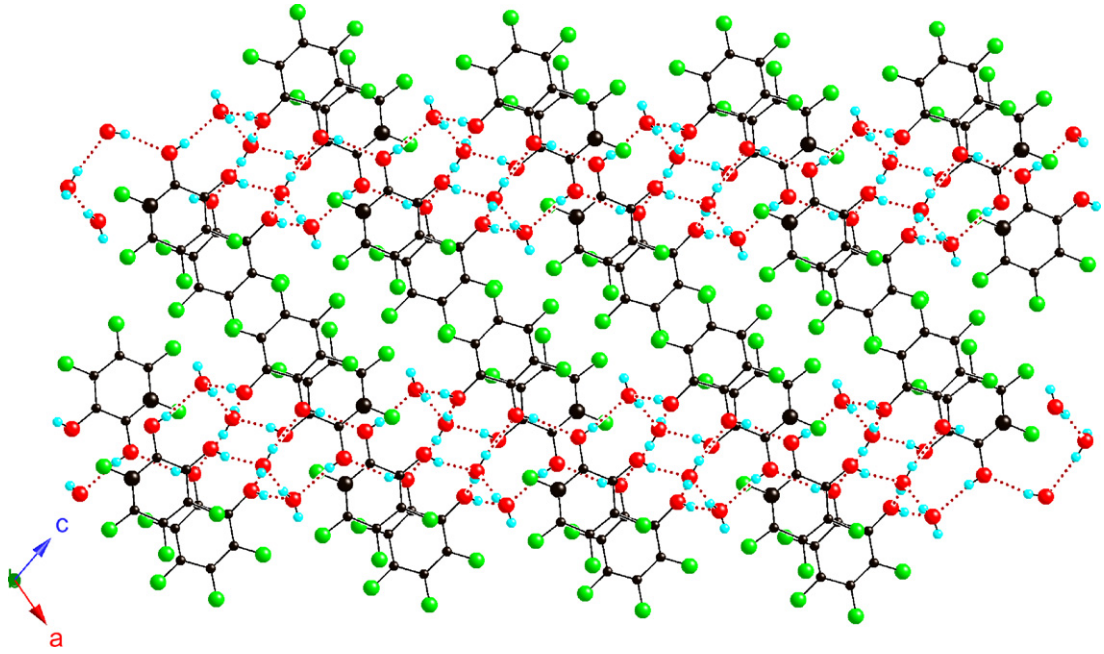

Fig. 6. Packing diagram for **3**·(H_2O).

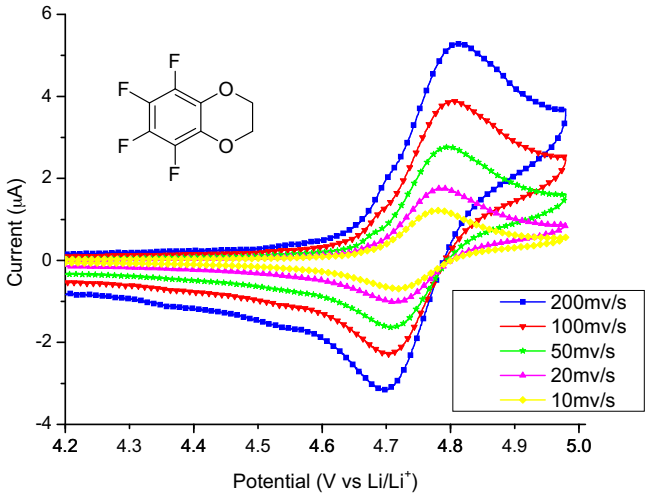

Fig. 7. Cyclic voltammograms for 0.05 M of **4** and 1.2 M $LiPF_6$ in EC/EMC (3/7 by volume) using Pt/Li/Li three-electrode cell.

redox potential of **4**, evaluated using the mean of the anodic and cathodic potentials [($E_a + E_p$)/2], is 4.75 V vs. Li/Li^+, which is high enough to provide overcharge protection for most positive electrode materials. To further explore the redox shuttle capability of **4**, overcharge testing experiments with 2032 coin cells are ongoing in our laboratory and the result will be reported in future.

3.4. DFT calculations

The 5,6,7,8-tetrafluoro-(1,4)-benzodioxane molecule (**4**) was optimized at the B3LYP/6-31G* level of theory, and its frequencies were calculated [13]. Selected optimized geometrical parameters are listed in Table 2. The calculated values are in good agreement with experiment, including the half-chair conformation of the 1,4-dioxane ring fused to the benzene ring. Calculated atomic charges show a stronger negative charge on oxygen of **4** (−0.74) than on F1 (−0.54) and F2 (−0.52), which is consistent with resonance donation of electrons by F.

We also calculated the oxidation potential of **4** at the B3LYP/631 + G (3df, 2p)//B3LYP/6-31G* level of theory relative to the lithium electrode. For this calculation we used the method

described in Ref. [14] for calculation of reduction potentials, except that we have derived the ionization potential by calculating the cation of 5,6,7,8-tetrafluoro-(1,4)-benzodioxane. The free energies in solution were calculated by using a continuum model, as described in Ref. [12]. The calculated potential is 4.68 eV, in good agreement with the experimentally measured value of 4.75 eV.

3.5. Synthesis and full characterization of PFPTFBB (**1**)

The synthesis of PFPTFBB from TFC and pentafluorobenzene boronic acid is shown in Scheme 1. In a typical dean-stark distillation setup, a mixture of TFC and the boronic acid in toluene is refluxed under N_2. The reaction is driven to completion by continuous removal of water byproduct from the reaction flask by azeotropic distillation. The crude product can be further purified by sublimation at reduced pressure. The ^{19}F NMR spectrum of **1** in d_6-DMSO (deuterated dimethyl sulfoxide) gave distinct resonances for five nonequivalent fluorines (Fig. 8). The ratio of the integration for ^{19}F resonance peaks is 2:2:2:2:1; this ratio is consistent with the structure assignment of PFPTFBB.

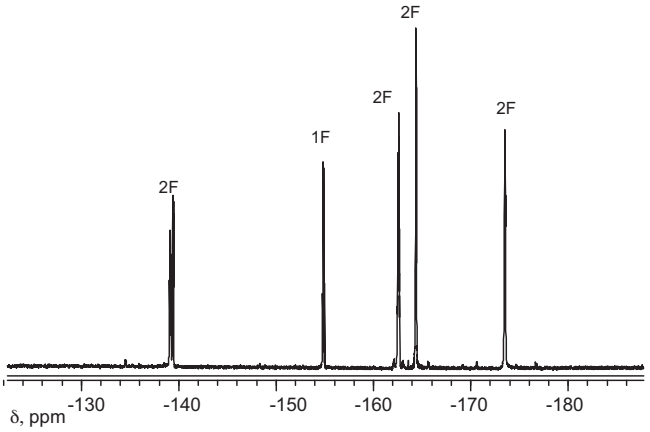

Fig. 8. ^{19}F NMR spectrum of PFPTFBB in d_6-DMSO.

Fig. 9 is the atmospheric pressure chemical ionization (APCI) negative ion mass spectrum of PFPTFBB. The typical peaks in the ESI-MS spectrum are $[M_{PFPTFBB}+Cl]^-$ (393.0), $[M_{TFC}-H]^-$ (181.0), $[M_{PFBBA}+Cl]^-$ (246.9), and $[M_{PFPTFBB}+M_{TFC}-H]^-$ (539.0). These results support the Lewis acidity and anion binding capability of the boron center. Decomposition ions of PFPTFBB were also observed and are probably due to its reaction with moisture. PFPTFBB is relatively moisture sensitive. Fig. 10 presents the cyclic voltammograms for 0.05 M of PFPTFBB from two batches in 1.2 M $LiPF_6$

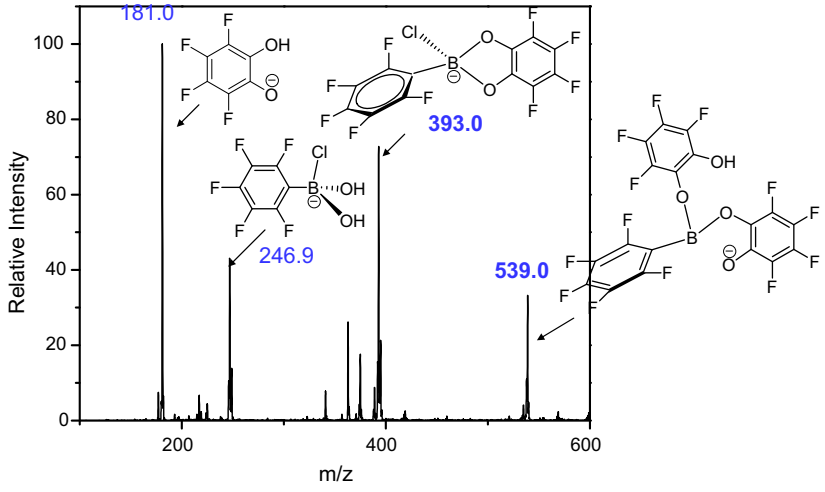

Fig. 9. ESI-MS spectrum of PFPTFBB (negative scan).

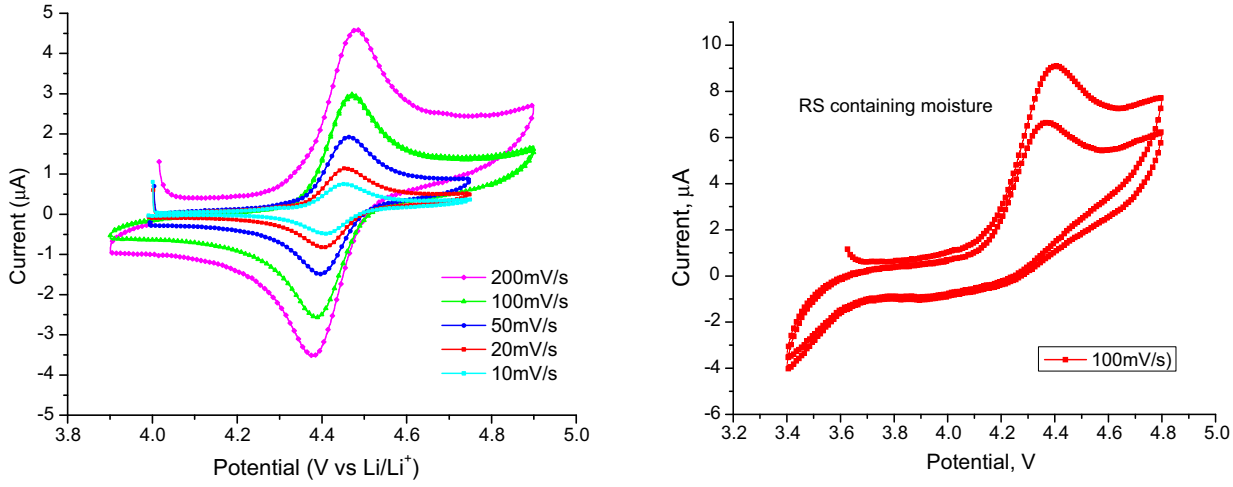

Fig. 10. Cyclic voltammograms for 0.05 M of PFPTFBB in 1.2 M $LiPF_6$ in EC/EMC (3/7 by volume) (left: PFPTFBB prepared under strict anhydrous condition; right: PFPTFBB exposed to air).

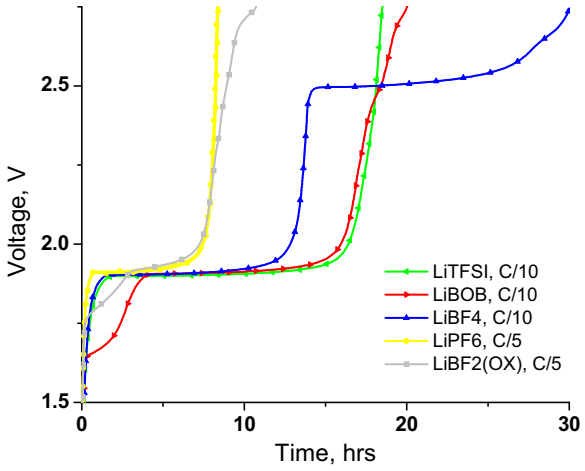

Fig. 11. Voltage profiles of LTO/$LiFePO_4$ cells containing 1% PFPTFBB in different electrolytes under constant rate charging.

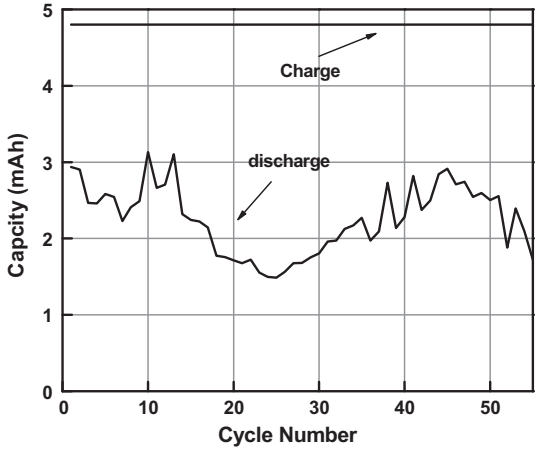

Fig. 12. Overcharge cycling performance of MCMB/$LiNi_{0.8}Co_{0.15}Al_{0.05}O_2$ cell. The electrolyte contains 3 wt% PFPTFBB and 1.5 wt% LiF.

in EC/EMC (3/7 by volume). When the reaction and purification step were carried out under strict anhydrous condition, the cyclic voltammetry curves are reversible (Fig. 10, left). When the compound was exposed to air, the cyclic voltammetry curves are irreversible (Fig. 10, right). This is probably caused by the irreversible oxidation of tetrafluorocatechol (formed by hydrolysis of **1**) to tetrafluoroquinone.

3.6. Overcharge test of PFPTFBB

The overcharge protection of PFPTFBB has been studied with various lithium salts in EC/EMC (3/7 by volume). The molarity of the lithium salt is 1.0 M except LiBOB, which is 0.5 M due to its lower solubility in carbonate solvents. For a quick comparison, overcharge tests were conducted with 2032 coin cells under constant current charging while monitoring the cell voltage. Fig. 11 shows the overcharge voltage profiles of LTO/$LiFePO_4$ cells with 1.0 wt% PFPTFBB in several prepared electrolytes. During charging of the LTO/$LiFePO_4$ cells, the lithium ion was removed from the $LiFePO_4$ positive electrode and intercalated into the LTO negative electrode. Only the cell with $LiBF_4$ displayed two distinct voltage plateaus with the first one at 1.9 V for the normal cell charge and the second one at about 2.5 V where the overcharge protection is activated.

Fig. 12 shows the charge/discharge capacity of a graphite MCMB (mesocarbon microbeads)/$LiNi_{0.8}Co_{0.15}Al_{0.05}O_2$ cell containing 3% PFPTFBB and 1.5% LiF in the electrolyte. The cell was charged and discharged at a constant current of *C*/10. The cell was charged to 4.98 V or until 4.8 mAh charge was delivered (100% overcharge). After more than 50 cycles, the overcharge protection of the redox shuttle was maintained, although the discharge capacity showed some fluctuation. The addition of LiF is believed to disfavor the decomposition of $LiPF_6$ to form LiF and PF_5. Surprisingly, the combination of PFPTFBB and LiF in $LiBF_4$-based electrolyte does not provide any overcharge protection.

4. Conclusions

3,4,5,6-Tetrafluorocatechol (**3**) was synthesized by a modified literature procedure with an improved yield. The challenge for the whole synthesis lies in the C–O cleavage step, in which the major byproduct bibenzyl is formed and is difficult to isolate from the desired product, even by sublimation. Flash chromatography seems the most effective method to isolate the product from biaryl byproduct due to their large difference in polarities. The intermediate compound **4** shows interesting electrochemical properties and great potential for overcharge protection of lithium-ion batteries. The crystal structures of both compounds contain fluorophillic interactions, while that of **3**·(H_2O) also has an extensive hydrogen-bonded network involving water molecules. Finally, we confirmed that PFPTFBB is a stable redox shuttle for overcharge protection for 4 V class lithium-ion batteries.

Supplementary data

X-ray crystallographic details, including selected bond lengths and angles, in CIF format. CCDC 768063 and 768064 contain the supplementary crystallographic data for compounds **3** and **4**, respectively. These data can be obtained free of charge from the Cambridge Crystallographic Data Center (via www.ccdc.cam.ac.uk/data_request/cif).

References

[1] H.S. Lee, X. Sun, X.Q. Yang, J. McBreen, J. Electrochem. Soc. 149 (2002) A1460.
[2] Z. Chen, K. Amine, Electrochem. Commun. 9 (2007) 703.
[3] J. Burdon, V.A. Damodaran, J.C. Tatlow, J. Chem. Soc. (1964) 763.
[4] C. Macdonald, A.J. Tomlinson, C.J. Willis, Can. J. Chem. 49 (1971) 2582.
[5] J. Barthel, R. Buestrich, E. Carl, H.J. Gores, J. Electrochem. Soc. 143 (1996) 3572.
[6] G.M. Sheldrick, SADABS, Version 2.03a, Bruker AXS, Inc., Madison, WI, USA, 2001.
[7] G.M. Sheldrick, SHELXTL, Version 6.12, Bruker AXS Inc., Madison, WI, USA, 2001.
[8] U. Haffer, W. Rotard, J. Pickardt, J. Fluorine Chem. 73 (1995) 265.
[9] D. Rainville, R.A. Zingaro, E.A. Meyers, Cryst. Struct. Commun. 9 (1980) 771.
[10] J.P. Jasinski, R.J. Butcher, H.S. Yathirajan, B. Narayana, L. Mallesha, K.N. Mohana, J. Chem. Cryst. 39 (2009) 453.
[11] O.J. Dautel, M. Fourmigué, J. Org. Chem. 65 (2000) 6479.
[12] K. Reichenbacher, H.I. Suss, J. Hulliger, Chem. Soc. Rev. 34 (2005) 22.
[13] M.J. Frisch, G.W. Trucks, H.B. Schlegel, G.E. Scuseria, M.A. Robb, J.R. Cheeseman, J.A. Montgomery Jr., T. Vreven, K.N. Kudin, J.C. Burant, J.M. Millam, S.S. Iyengar, J. Tomasi, V. Barone, B. Mennucci, M. Cossi, G. Scalmani, N. Rega, G.A. Petersson, H. Nakatsuji, M. Hada, M. Ehara, K. Toyota, R. Fukuda, J. Hasegawa, M. Ishida, T. Nakajima, Y. Honda, O. Kitao, H. Nakai, M. Klene, X. Li, J.E. Knox, H.P. Hratchian, J.B. Cross, V. Bakken, C. Adamo, J. Jaramillo, R. Gomperts, R.E. Stratmann, O. Yazyev, A.J. Austin, R. Cammi, C. Pomelli, J.W. Ochterski, P.Y. Ayala, K. Morokuma, G.A. Voth, P. Salvador, J.J. Dannenberg, V.G. Zakrzewski, S. Dapprich, A.D. Daniels, M.C. Strain, O. Farkas, D.K. Malick, A.D. Rabuck, K. Raghavachari, J.B. Foresman, J.V. Ortiz, Q. Cui, A.G. Baboul, S. Clifford, J. Cioslowski, B.B. Stefanov, G. Liu, A. Liashenko, P. Piskorz, I. Komaromi, R.L. Martin, D.J. Fox, T. Keith, M.A. Al-Laham, C.Y. Peng, A. Nanayakkara, M. Challacombe, P.M.W. Gill, B. Johnson, W. Chen, M.W. Wong, C. Gonzalez, J.A. Pople, Gaussian 03, Revision C. 02, Gaussian, Inc., Wallingford, CT, 2004.
[14] J.M. Vollmer, L.A. Curtiss, D.R. Vissers, K. Amine, J. Electrochem. Soc. 151 (2004) A178.